# Behavior of Steel Structures against Blast Load – Design of energy dissipation systems

José André Ricardo Pinto
598pinto@gmail.com
IST, Technical University of Lisbon, Portugal
AM, Military Academy, Portugal

## Abstract

Nowadays, there are many vectors on terrorist action in the society, being explosive devices one of the most used means of attack on the population and critical infrastructures. Civil engineering has the responsibility of designing structures to withstand a wide range of effects, including the effects of explosions from terrorist activities.

When a steel structure is subject to the effects of an explosion, the columns are the most vulnerable structural element. This study presents the behavior of steel structures under explosive actions and the design of a simple, efficient and economical energy dissipation device with high energy absorption capacity, which aims to minimize the amount of energy impacting on the main structure.

Based on commercial steel profiles, the dissipation devices connect the coating system to the main structure. They allow energy dissipation through material plastification and profit from steel resistance increase for high strain rates. The development of these devices was supported by numerical modeling of their behavior during the blast load propagation using the LS-DYNA software.

The concept of energy dissipation was observed throughout the study of the dissipation system. It was possible to conclude that the main parameter in the first phase of action is the device inertia, and the strain rate sensitivity is the main parameter in the second phase, allied to a continuous dissipation of energy by rotation at the plastic hinges.

**Keywords:** Explosion action, Energy dissipation, Steel column, Dissipation efficiency; Absorption of energy; Plastification of steel elements.

## 1.Introduction

The evolution of construction is associated with causes and effects of the environment to which we are subjected. For many years, mankind has needed to seek safety and shelter, developing techniques and procedures to ensure protection and structural integrity. Many types of actions, such as wind, thermal actions, seismic events and gravity loads, should be considered in structural design. However, accidental actions, such as blast explosions, are gaining importance in modern times (e.g. in the chemical industry, or airport facilities).

Alongside the development of protection capability, the destruction capacity has also increased. The phenomenon of terrorism is not new, although it was believed that some limits would not be exceeded, such as the ones witnessed in recent times, including suicide bombings and mass massacres.

In April 19, 1995 occurred one of the biggest terrorist attacks in US history, an undercover bomb truck with approximately 2200 kg of ANFO (Ammonium Nitrate / Fuel Oil) exploded at about five meters from the north facade of the Federal Building Alfred P. Murrah (a reinforced concrete structure), causing 168 deaths (87% due to collapsed debris) and surrounding damages equivalent to a loss of approximately 50 million dollars. The blast destroyed the columns of the first floor which supported a transfer girder with a 12-meter span (**Figure 1**).

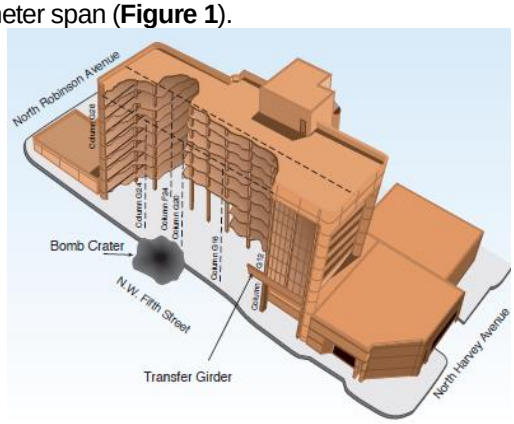


**Figure 1:** Murrah building after the attack. The front face portion gradually collapsed [1]

Although no terrorist attack has occurred in Portugal after the dismantling of the terrorist group FP25 in the 80s of the last century, there is an medium terrorist threat according to the Portugal

internal security Annual Report of 2017 [2]. Given the uncertainty that prevails and the need to design structures for very long-life cycles, it becomes relevant to discuss and study methodologies to enhance the protection of facilities, whether military or civilian.

Steel construction has shown a positive dynamic behavior even in time of economic crisis. Steel meets the sustainability criteria and reduces the construction work impacts. It is also very adaptable and 100% recyclable, managing to ensure the dynamics in which we live, with tight deadlines coupled with the satisfaction guarantee.

However, knowledge of the behavior of steel structures under blast actions is still limited, thus this work aims to expand knowledge at the level of structural response of steel structures under the action of an explosion.

In Portugal, research conditions for studying the explosive action effects are costly, and therefore, they are mostly restricted to the armed forces. The "Centro de Competências para a Proteção de Infraestruturas" (CCPI), which includes, also, members from Instituto Superior Técnico and Faculdade de Ciências e Tecnologia da Universidade Nova de Lisboa, is dedicated to this research and the investigation of solutions to enhance the resilience of military and civilian infrastructures.

## 2.Blast effects

An explosion can be simply defined as a large and sudden release of energy [3]. It may also be defined as a big environment change, in a short time lap of time, which creates the release of gas and a large amount of energy, usually in the form of heat, leading to the formation of blast waves (high pressure).

The drop of pressure over time (**Figure 2**) is represented by the modified equation of Friedlander (1):

$$P_s(t) = P_{so} \times \left(1 - \frac{t}{t_0}\right) e^{-b\frac{t}{t_0}} \quad (1)$$

where, $P_{so}$ [kPa] is the peak incident pressure, $t_o$ [ms] is the duration of the positive phase, $t$ [ms] is the time period between the time of arrival ($t_a$) and the instant in which we want to carry out the analysis, and $b$ is the curve's decay coefficient [7].

### 2.1 Explosion parameters

#### a) Equivalent TNT weight

To define the parameters of an explosion, the TNT equivalent weight must be obtained by Eq. 2:

$$W_{TNTe} = \frac{H^d_{EXP}}{H^d_{TNT}} \times W_{EXP} \quad (2)$$

where, $W_{TNTe}$ represents the equivalent mass of TNT, $W_{EXP}$ is the explosive mass in study, $H^d_{EXP}$ the blast heat from the explosive in study and $H^d_{TNT}$ the blast heat of TNT.

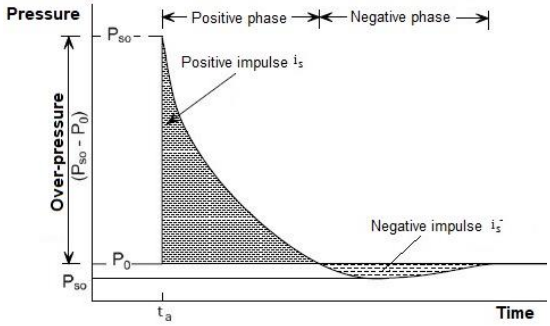


**Figure 2:** Idealized profile pressures, adapted from [8]

#### b) Scaled distance

The shock wave propagation is generally described in terms of the parameter $Z$, the scaled distance. This parameter indicates that, for the same scaled distance and detonation in the same environment, two loads of the same type of explosive with the same geometry but different size, originate equal shock waves. This relationship formulated by Hopkinson Cranz, 1915 and 1926 respectively, is defined by Eq. 3:

$$Z = \frac{R}{\sqrt[3]{W}}, \quad (3)$$

being $Z$ the scaled distance $\left[m/kg^{\frac{1}{3}}\right]$, $R$ the distance between the target surface and the epicenter of the explosive charge [$m$], and $W$ the mass of the explosive charge [$kg$] [4], [9].

#### c) Peak incident pressure

Several authors have presented formulas for peak incident pressure. The formulation by Kinney and Graham [5] will be used for the definition of the incident peak pressure [$MPa$], given by Eq. 4:

$$P_{so}[MPa] = \frac{808\times\left[1+\left(\frac{Z}{4,5}\right)^2\right]\times P_0}{\left[1+\left(\frac{Z}{0,048}\right)^2\right]^{\frac{1}{2}}\times\left[1+\left(\frac{Z}{0,32}\right)^2\right]^{\frac{1}{2}}\times\left[1+\left(\frac{Z}{1,35}\right)^2\right]^{\frac{1}{2}}} \quad (4)$$

#### d) Positive phase duration

The damage inflicted in a structure largely depends on the load application time duration due to explosion. This load application time is correlated with the time of the positive phase [$ms$]. Eq. 5 proposed by Kinney and Graham [5] gives the positive phase duration ($t_0$):

$$t_0[ms] = \frac{980\times\left[1+\left(\frac{Z}{0,54}\right)^{10}\right]\times\sqrt[3]{W}}{\left[1+\left(\frac{Z}{0,02}\right)^3\right]\left[1+\left(\frac{Z}{0,74}\right)^6\right]\left[1+\left(\frac{Z}{6,9}\right)^2\right]^{\frac{1}{2}}} \quad (5)$$

The resulting thrust of the blast action is given by the integral of the pressure curve.

#### e) Shock wave reflection

Reflection and amplification occur when the shock wave hits a solid surface (**Figure 3**). The reflected peak pressure $P_r$, given by Eq. 6, is always higher than the incident peak pressure $P_{so}$.

$$P_r\,[MPa] = 2 \cdot P_{so} \times \left(\frac{7 \cdot P_o + 4 \cdot P_{so}}{7 \cdot P_o + P_{so}}\right) \quad (6)$$

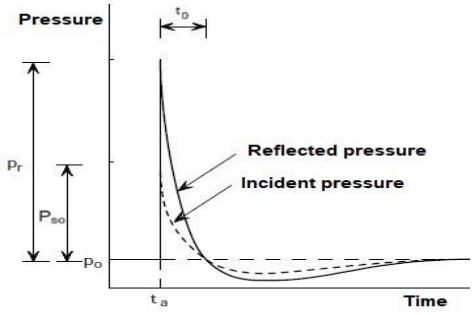


**Figure 3:** Blast pressure evolution during time

## 2.2 Dynamic steel properties

Typically, steel exhibits higher resistance when subjected to high strain rates (**Figure 4**). The larger the deformation rate ($\dot{\varepsilon}$) by imposed loading, the less time there is to achieve the yielding point, and the greater will be the increase of strength capacity on the structural member. To account for this effect, a dynamic increase factor (DIF) is applied.

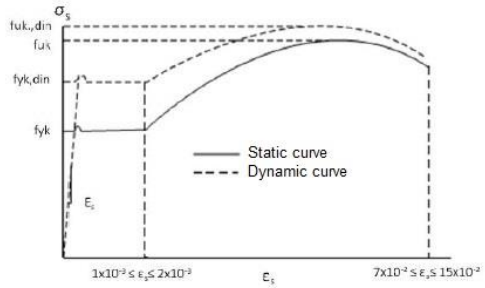


**Figure 4:** Typical stress-strain steel curve (adapt. from [8]).

**Figure 5** represents the expected deformation rates according to different applied actions. For a quasi-static regime, a deformation speed of, approximately, $10^{-6}\,s^{-1}$ can be observed and compared to a value of $10^{4}\ s^{-1}$ in the range for explosion [3]. To consider this behavior, the design yield stress ($\sigma_{y,dim}$) for a dynamic action, which causes bending in the structural element is given by the Eq. 7:

$$\sigma_{y,dim} = SIF \cdot (DIF) \cdot \sigma_y \quad (7)$$

where $SIF$ is a correction factor due to the yield stress of a structural element usually being greater than the minimum specified. For S275 and S355 steel, $SIF = 1.10$ [8].

The model of deformation rates proposed by Cowper-Symonds, Eq. 8 can be used to determine the dynamic increase factor:

$$DIF = 1 + \left(\frac{\dot{\varepsilon}}{D}\right)^{\frac{1}{q}} \quad (8)$$

Where $\dot{\varepsilon}$ is the strain rate, $D$ and $q$ are constant for the material. For the steel, $D = 40{,}00002\ s^{-1}$ and $q = 5$ [10].

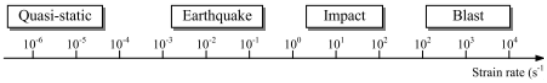


**Figure 5:** Strain rates associated with different types of loading, (adapt. from [3]).

# 3.Dissipative energy devices

Calladine and English [11] identified two general types of dissipative energy devices through plastic deformation. The two types are distinguished by its load-deformation curve: Type I is an example of a bilinear behavior, whereas Type II is an example of a curve with an initial peak and exponential decay, as illustrated in **Figure 6**.

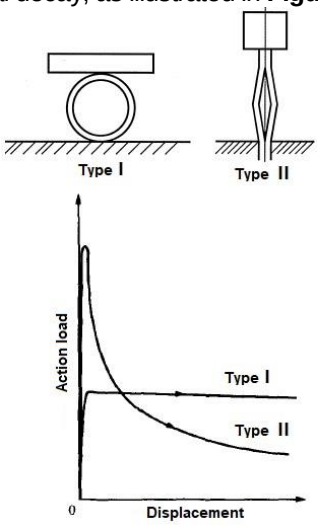


**Figure 6:** Types of dissipative energy devices with respective load-displacement curve.

Zhang and Yu [12] tried to present an analytical solution for the model by explaining the phenomenon. Tam e Calladine [13] conducted an analytical and experimental investigation, leading to key conclusions for future studies. According to these authors, Type I structures absorb energy linearly with displacement because the rotation in the plastic hinge is roughly proportional to deformation. However, due to the existing geometry in Type II structures, a large amount of energy is absorbed for a small deformation. The early stage phenomenon (mass impact) of Type II structures is detailed through an elastic-plastic model in Karagiozova and Jones papers [14], [15].

Su et al. [16], [17] studied the existing energy in each experimental phase, showing that the peak resistance in the specimen is obtained with the combination of high strain rate and high inertia, resulting in smaller displacements.

# 4.Calibration of the finite element model

The validation of the model was performed using the experimental and numerical studies of Nassr et al. on steel sections W [18]–[21]. The experimental tests used to calibrate the numerical models were obtained from the test program conducted by Nassr et al. in 2011 [19].

The experiment of a W150x24 column section placed at 9.0 m apart from the explosive load (250 kg of ANFO, equivalent to a scaled distance of 1.69 $m/kg^{\frac{1}{3}}$) was used. The column was modeled with shell elements (ELFORM16 and ELFORM2, respectively formulation fully integrated and Belytschko-Tsay,) with MAT_003-PLASTIC_KINEMATIC material, with $RO = 7850\ kg/m^3$, $E = 210\ GPa$, $PR = 0.3$, $SIGY = 470\ MPa$, $SRC = 40.00002\ s^{-1}$, $SRP = 5$ and $FS = 0.2$.

The column was modeled with a fixed support at the upper end, with all displacements and rotations prevented ($\delta_x = \delta_y = \delta_z = 0$, $\theta_y = \theta_z = 0$) except for rotation in $x$, and a roller support on the opposite end with free displacement along $z$ and rotation in $x$ ($\delta_x = \delta_y = 0$, $\theta_y = \theta_z = 0$). A rigid plate is modeled at each end of the steel column (MAT_020-RIGID) by using the boundary conditions mentioned above in the upper and lower face of each plate.

Three different meshes were used in the model and the resulting displacements were registered in **Figure 7**. The coarse mesh model showed a displacement at mid span of 30.44 mm, equivalent to a 1.50% error compared to the results of Nassr et al. (**Figure 8**). Since the error is small, this methodology was considered suitable for modeling real cases and new simulations.

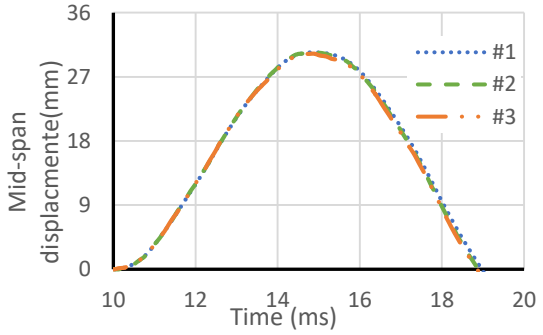


**Figure 7**: Mid span displacement for different meshes

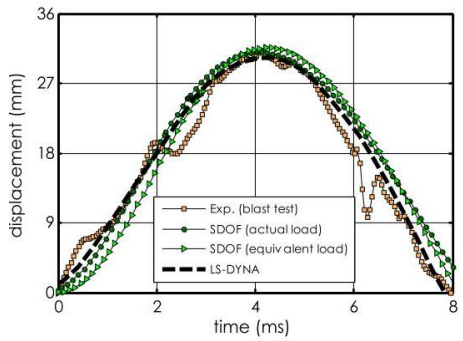


**Figure 8**: Mid span displacement obtained by Nassr et al. [18]

## 5.Case study

The steel structure consisting of columns with 3.0 meter of height IPE200 sections spaced by 2.0 meters was adopted. Facade sheet profiles cover the main structure. Different dissipation devices link the facade to the main column.

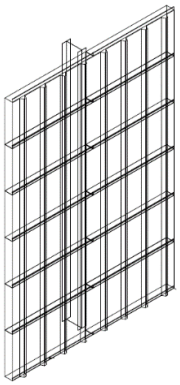

**Figure 9:** Model geometry.

All elements are made of steel, simply changing the yield point between them. For the profile and profiled sheet, $SIGY = 275\ MPa$ and for the facade profiles, $SIGY = 320\ MPa$. Shell elements were used with ELFORM2.

The links were modeled by welding points. The material is defined by MAT_100-SPOTWELD with beam elements (ELFORM 9).

For shell bonding and the welding points, *CONTACT_AUTOMATIC_ONE_WAY_SURFACE_TO_SURFACE and *CONTACT_SPOTWELD were used, respectively.

Two tests were considered for the same explosive load (**Figure 10**) of 3.0 kg of TNT. Both explosive loads E1 and E2 are set at 1.8 meters from the profiled sheet and 1.5 meters from the ground. The E1 test has the explosive load aligned with the profile, while the E2 test is aligned in between the profiles.

The model was performed by profiting from symmetry of the structure, with restricted displacement in $x$ ($\delta_x = 0$) and rotations on y and z ($\theta_y = \theta_z = 0$) in all nodes at the ends of the profiled sheet and facade profiles. The explosive load was modeled using card BLAST_ENHANCED.

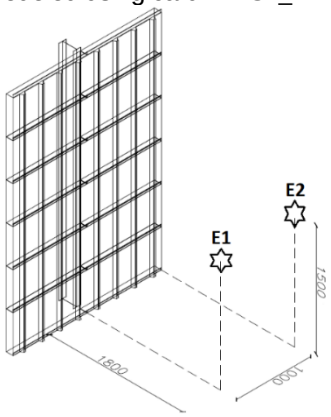


**Figure 10:** Scheme of E1 and E2 tests.

On a positive phase time of 2.47 ms, the modeled explosion produces an incident peak

pressure $P_{so} = 581\,kPa$ and a reflected peak pressure $P_r = 2245\,kPa$.

For the E1 test, the profile achieves a deflection of 89 mm (web) at 18 ms, with local plastic deformations on the mid-span. **Figure 11** shows the web displacement for the most critical section and the time curve of the blast action, measured at the receiving facade (profiled sheet). A qualitative representation of the time curve of the explosion (BLAST) is important to understand the time interval between the end of the action and the profile response.

After reaching the first higher deformation, the profile has a sinusoidal behavior until its final deformed configuration, with 74 mm of residual deformation. **Figure 12** presents the final plastic deformation (red) of the profile.

On E2 test, the residual displacement was 44 mm, showing a similar behavior to E1 test. Since the E2 test is the least demanding for the structure, only the E1 results are presented.

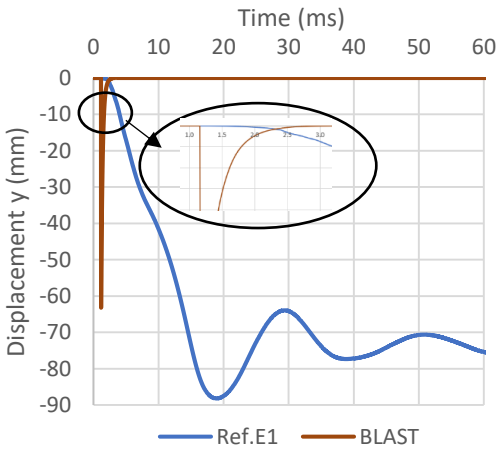


**Figure 11:** Displacement curve of the test Ref.E1.

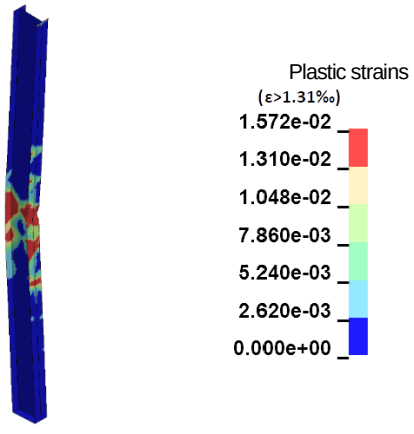


**Figure 12:** Plastic deformation in the reference test.

## 6.Design of energy dissipater device

An energy dissipater device has the purpose of reducing the energy transmitted to the structure. The effective energy dissipation is related to the time that the specimen must deform. The extent of deformation time means a greater power of dissipation (by means of plastic deformations) [22].

The goal is to design an energy dissipater device using standard steel profiles with the following capabilities:

- Plastic deformation distributed over the entire area and not just locally;
- Forecast of plastic deformation points combined with a good response across the whole blast spectrum;
- Continuous deformation until the end of the blast event;
- During the loading period, the devices must be able to dissipate energy through plastic deformations, contributing to a linear behavior of the structuring profile;
- Easy application on site.

According to Tam and Calladine [13] there are two response phases for the types of dissipater devices that will be presented. In the first phase, plastification occurs only due to the compression of the device, while in the second phase there is rotation of the plastic hinges. They also indicate that the dominant factor for the first phase is inertia, while for the second phase, it's the deformation rate.

At first, it was important to determine the results' analysis criteria so there would be a consistent parameter for the development of the study. For the steel device, energy dissipation through the formation of plastic hinges is expected, i.e. the more plastic deformations, the greater the released energy and, consequently, less energy is transmitted to a structural column.

The results obtained for the C1 devices are not referred to due to poor performance. Instability phenomena occurred, existing torsion in the device, which led to cracking and tearing of the steel walls. Despite causing torsion of the web, the S1 device contributed to a significant reduction of the displacements in the column. Results were reduced to, approximately, one third of the ones obtained without any type of dissipater device.

Given these two results, a study of different geometries based on the previous two sections was developed. The diagram illustrated in **Figure 13** represents, from top to bottom, advances in time performed at the level of the geometry of different dissipater devices.

The devices were divided into 4 groups: 1) commercial profiles; 2) unstable profiles; 3) profiles with a thickness of 4mm; and 4) sheet plate/profiled sheet.

Group 1 consists on C1 - CHS 60.3x 5.0 mm and S1 - SHS 100x100x4.0 mm profiles. The second group consists of the profile C1 and C2 (C1 variant by introducing a longitudinal cut). The third group is defined by elements derived from

commercial profiles with a constant thickness of 4 mm and will be used for result comparison. Finally, the fourth group consists of devices made by cold bending of thin plates.

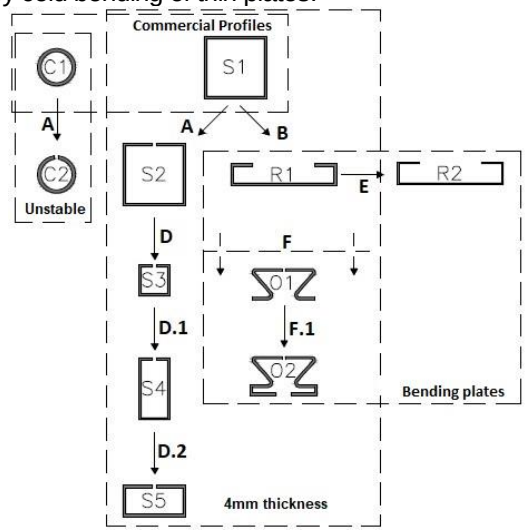


**Figure 13:** Timeline of the design of the dissipater devices.

The stages of development represented alphabetically in **Figure 13** are:

- **A:** Performing a cut of 6 mm in the face oriented to the blast. The cut tries to reduce instability in C1 device. Although improvement on stability due to horizontal pull was expected after the introduction of the opening section, this was not the case. On the other hand, the quadrangular section dissipater devices are expected to increase flexibility in the system, since the behavior of the profile and the S1 device is monolithic. The cut (S2) weakens the system, removing the monolithic behavior from the structure, where the device behaves as two independent webs and a flange for connection to IPE200. In theory, this leads to two new plastic hinges represented by the connection flange device - flange profile;
- **B:** Creation of side "tabs" (exterior to the flange of the IPE200) maintaining the amount of material by reducing the depth of the solution. This solution appeared simultaneously with S2;
- **D:** Reduction of the section to half while maintaining the S2 study scheme. Since the cost of a solution is an important factor of choice and validation, the section was reduced from 100x100x4.0 mm (S2) to 50x50x4.0 mm (S3);
- **D.1, D.2:** Study of rectangular solutions merging geometries from S2 and S3 devices and obtaining sections 50x100x4.0 mm (S4) and 100x50x4.0 mm (S5);
- **E:** Study of the influence of the plate thickness. Since there are no commercial profiles 2.0 mm thick, the study of the thickness influence focused in steel sheet R1, reducing from 4.0 to 2.0 mm (R2), aiming to understand if there is still enough deformation capacity when reducing the thickness;
- **F, F.1:** Predicting the deformation points. Through the bending of a plate with the presented geometry, it is possible to predict the position of plastic hinges. After the above steps, O2 device becomes innovative when compared with the previous systems, since it contains fastening tabs to the flanges, adjustable according to the thickness of the structural profile flange. With the creation of locking tabs and through self-tapping screws, it is possible to install the bolt from the 'protected side' of the flange (relative to the origin considered in the tests). This creates two additional dissipation points at flange ends, which results in the bolt being the last point of rotation of the solution.

### 6.1 Test S1

The use of energy dissipaters causes the first inflection point to occur earlier, obtaining a maximum elastic displacement of 36 mm in comparison with 89 mm recorded in the reference test. After this inflection point, the profile has, approximately, a sinusoidal behavior with a residual displacement of 22 mm compared with 75 mm for the reference test (**Figure 14**).

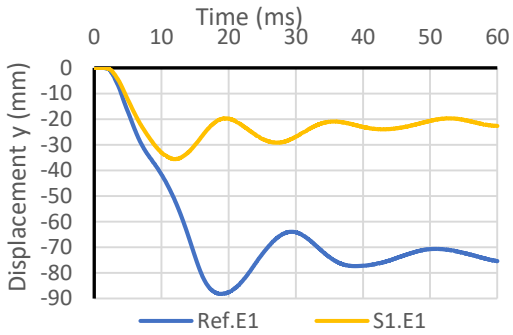


**Figure 14:** S1.E1 displacement curve compared to Ref.E1.

### 6.2 Tests S2, S3, S4 and S5

It is intended to investigate how the section geometry openings affect the global behavior. In these devices, it is expected that the effects in the second phase of action, corresponding to rotation at the hinge's points, are attenuated by the device flexibility. **Figure 15** shows displacement curves for tests S1.E1 to S5.E1.

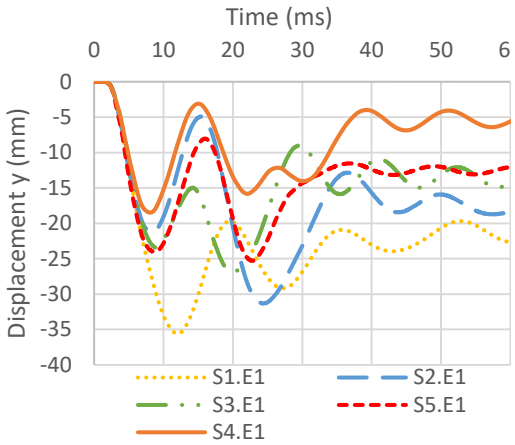


**Figure 15**: Displacement curve of S1.E1 to S5.E1 trials

It is important to note that all devices with openings are more flexible, therefore, they dissipated more energy, allowing a reduction of the mid-span displacement when compared to S1. Moreover, it is noted that the first inflection point occurs prior to the assay closed device. In conclusion, there is an improvement in the response of the assembly, allowing a high-power dissipation with low energy transfer to the profile.

At the end of analysis, S2 is the device with greater residual deflection.

From this study, it is concluded that the best configuration comprises a short flange and high web heights, which allow a good initial response to compression and produces well-defined rotations around the plastic hinges, allowing continuous deformation of the dissipater's flange. With the S4 configuration, a decrease of the residual displacement was achieved, obtaining a reduction from 75 mm to approximately 5 mm (i.e., 93.3%). **Figure 16** presents the initial state (the first inflection point) and final deformation of S4 device.

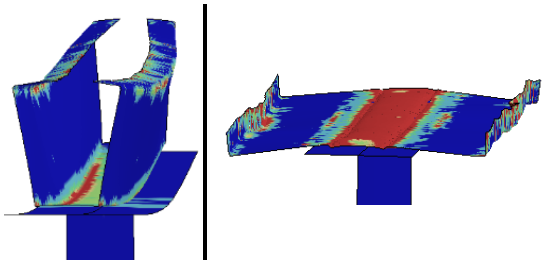

**Figure 16:** Initial state, the left (first point of inflection), and final state, the right, the S4 device

### 6.3 R1 and R2 tests

R1 test is characterized by a modification of S1 / S2, seeking to increase system flexibility by adding a 'flap', when compared to the IPE200 flange. **Figure 17** shows the increase of the device flange relative to the profile flange. Maintaining the mass of the S2 device, R1 creates a possible configuration by cold forming with two additional hinge points, which are predicted to occur at the IPE200 flange attachment.

R2 device is used to understand how the plate thickness influences the overall behavior of the combination (IPE200 + dissipater device). This new configuration, with a reduced thickness, evidenced the worst behavior expected, since the mass of the system is relevant to the explosion.

**Figure 18** shows the displacement curves for the test S2, R1 and R2. The behavior of the R2 is far from desirable. Analyzing device R2, it is proven that the thickness, and, therefore, the mass of the device, contributes efficiently to the overall response.

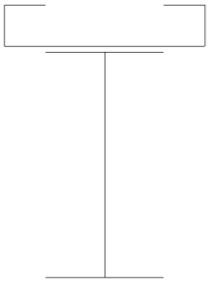

**Figure 17:** Device R1, design of 'tabs'.

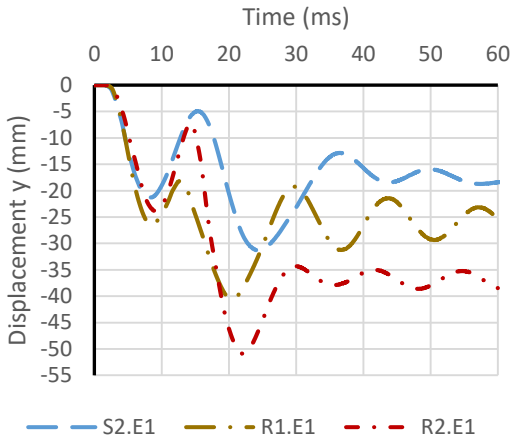


**Figure 18:** Displacement curves of S2.E1, R1.E1 e R2.E1.

R2 device had the opposite behavior of what was required for this type of elements. On the initial impact, the device presented a fully plastic behavior due to reduced inertia, lacking reserves for a required continuous response.

Both cases (R1 and R2) have a similar behavior, poor than the previous solutions.

### 6.4 Innovative devices O1 and O2

The device O1, with the omega shape (Ω) from **Figure 13**, was a first attempt to create a device that could dissipate the maximum energy during the blast action. The omega section aims to provide a good resistance to the initial impact, in which a considerable inertia is required, and aims to add predictable plastic hinges for a good response in the second phase of the action, hoping to get a continuous response over time. An improvement of this behavior was achieved using O2 omega shape device. The innovation in this device is the creation of laterals fittings which can

be used throughout the flanges spectrum by changing the thickness of the fitting. Thus, the flange of IPE200 and the Omega device work together in the first phase of the action. In the second phase of action, a continuous response is guaranteed by adding more plastic hinges. The connection of the O2 device is made from the inner side of the IPE200 flanges, which can be achieved in the construction site with self-tapping screws. **Figure 19** illustrates the expected mechanism for this device during the blast action.

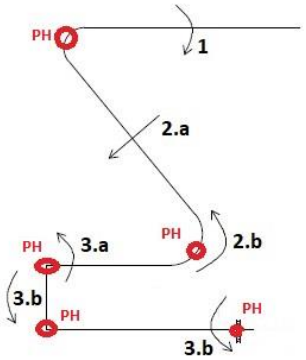


**Figure 19:** Expected mechanism of device O2.

**Figure 19** corresponds to the formation of **PH –** Plastic hinge with the following sequence:

- **1 –** Flange rotation due to the initial impact;
- **2.a** and **2.b –** the inclined web tends to move in the direction presented after initial impact, therefore, there is a rotation (2b). It is expected energy dissipation in RP before the occurrence of rotation 2b;
- **3.a** and **3.b –** These rotations are expected almost simultaneously with a high concentration of tensions between the rotation 3.a and 3.b. The self-tapping screw is considered to be the last point of rotation of the whole body. The three lower PH are designed to allow the continuous deformation of the device.

**Table 1** displays the geometric proper-ties of the O2 section device.

**Table 1:** Geometric properties of O2 device.

| | $I_x[mm^4]$ | $i_x[mm]$ | $i_y[mm]$ | $i_x/i_y$ |
|---|---|---|---|---|
| **O2** | $394{,}7 \times 10^3$ | 23,29 | 12,35 | 1,64 |

**Figure 20** shows the displacement curves of S2 (reference), S4 (the best of the above) and O2 devices. Analyzing the second inflection point of the curves shown in **Figure 20**, O2 nearly allows a 100% recovery of the profile, with larger waves. The final behavior is similar to S4 device. The deformations in the first three inflection points are represented in **Figure 21**.

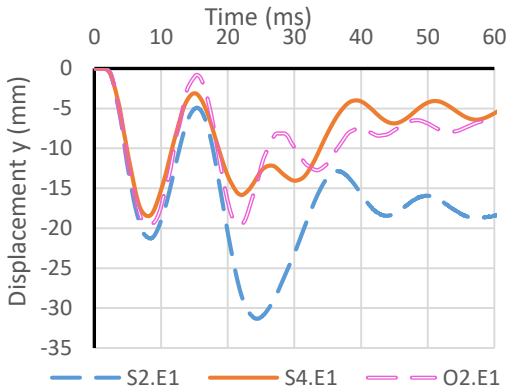


**Figure 20:** Displacement curves of S2.E1, S4.E1 and O2.E1

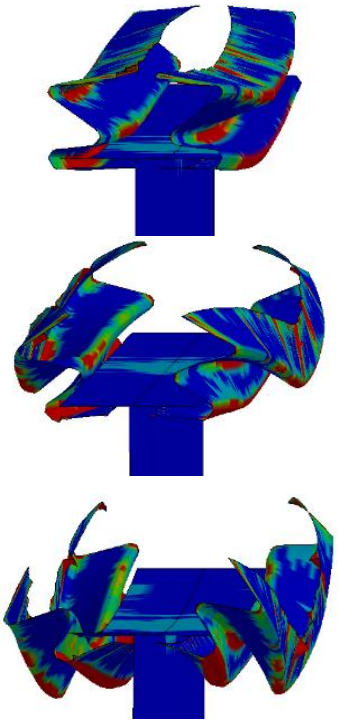

**Figure 21:** Behavior O2 device, inflection point 1,2 and 3 respectively

### 6.5 Blast spectrum study

As shown earlier in this chapter, for a steel device to be considered effective, it must be able to respond identically to the whole blast spectrum. Therefore, this section aims to study the behavior of devices S2, S3, S4 and S5, by applying representative blast loads with scaled distances close to a unit. The smaller the scaled distance the greater the blast.

The study with scaled distances below the unit is not recommended due to turbulence. Thus, a total of 16 models were carried out, of which 4 have already been presented (E1 tests mentioned above). The distance from the center of the explosion to the coating was used as the variable parameter, keeping the explosive load mass of 3.0 kg. The test has a distance from the steel coating of 1.8 m, which correspond to a scaled

distance $Z = 1.248\ [m/kg^3]$. **Table 2** shows the scaled distances associated with each test.

**Table 2:** Scaled distance $Z$ depending of the distance ($R$)

| $R$ | $1.8m$ | $1.7m$ | $1.6m$ | $1.5m$ |
|---|---|---|---|---|
| $Z[m/kg^3]$ | 1.248 | 1.179 | 1.109 | 1.040 |

Even with increase of blast energy, none of devices failed, which a very satisfactory result taking into consideration the load increase. **Figure 22** shows the residual displacements for each case. These results show a high energy dissipation capacity obtained for a wide spectrum of blast action. Device S4 presented the best results.

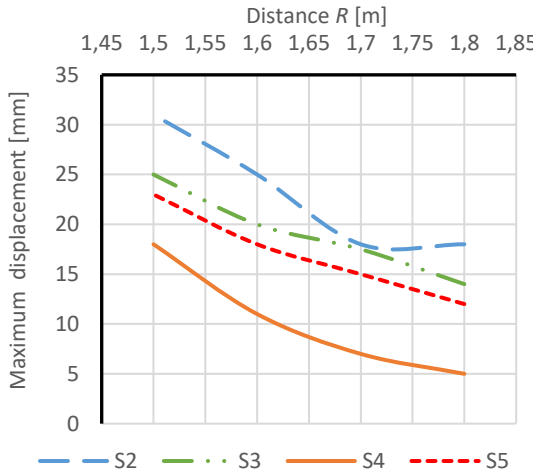


**Figure 22:** Residual displacements on the blast spectrum for various values of the blast distance, *R*.

### 6.6 Device's efficiency

The software registers the existing energy (kinetic, internal, etc.) in different parts of the system through the card *DATABASE_MATSUM. The internal energy of an element is directly related to its plastic deformations. Therefore, when low internal energy is achieved, the main structure specimen will present small plastic deformations and thus low residual displacements.

The internal energy of the device element is not the most accurate parameter to assess, since local plastic deformations occur and do not contribute for energy dissipation of the structure. Thus, the efficiency evaluation of each device is made according to internal energy of the flanges and web of the main structure profile, with and without the energy dissipater device.

The efficiency of each device ($\eta$) is given by Eq. 9, where $E_{i,device}$ is the internal energy of the IPE200 with device and $E_{i,reference}$ is the internal energy of the reference test, without the device:

$$\eta[\%] = 1 - \frac{E_{i,device}}{E_{i,reference}} \qquad (9)$$

**Table 3** presents the efficiency of each device on preventing plastifications of the IPE200 web and flanges. It is easily concluded that the S4 device S4 the most efficient.

**Table 3:** Device's efficiency

| Internal energy | S2 | S3 | S4 | S5 | O2 |
|---|---|---|---|---|---|
| **Web** | 66% | 70% | 82% | 73% | 79% |
| **Flanges** | 68% | 73% | 85% | 75% | 80% |
| **IPE200 (web + flange)** | 68% | 73% | 84% | 75% | 80% |

## 7.Summary and conclusions

The design of the dissipater devices was planned as a basic concept of the CCPI, seeking simple solutions for complex problems. These devices started out as commercial profiles and were changed by adding cuts and bending plates.

The behavior of a protection system must always consider three factors: the device, the structural element and the blast action.

In this research, two factors were kept constant: the structural element and the action, being the dissipater device the investigation topic. Thus, the conclusions must only be applied for the IPE200 column subjected to the defined action. However, the key points set below are valid when designing any steel dissipater device:

- As in Calladine and English studies [11], it was observed that the inertia of the device, in the direction of action, is the most important parameter in the first phase of the blast explosion;
- High deformation rates associated with explosions must be dissipated through steel elements profiting from theirs increased resistance, allowing plastic deformations without reaching failure at the first impact;
- For devices with long webs applied on the flange of the IPE200, the smaller the flange length of the device, the better its initial performance, since it is supported by a more rigid base of the profile flange, which results in better behavior;
- Devices with short flanges show better behavior when combined with long webs;
- It's essential to be able to predict the collapse mechanism through formation of well-defined plastic hinges;
- The energy dissipated in the plastic hinges is more important than the web's plastic deformation;
- Greater web rotations result in higher energy dissipation;

- The longer the energy is dissipated, the lower the final deformation of the structural element. Thus, continuous release of energy is very advantageous.

**Table 4** presents various relevant aspects for the choice of a dissipater device, marked these important factors with a score from 1 to 3 (1-bad, 2-acceptable, 3-good), based on the performance of each device. Since some of the topics under study are not easy to evaluate for device O2, it was not included in the table.

From this research study, device S4 presents the best behavior. Apart from having the best total score, it is also globally more efficient. Its characteristics have enabled a continuous response during time to a high response spectrum.

**Table 4:** Dissipater devices comparative table

| Parameter | S2 | S3 | S4 | S5 |
|---|---|---|---|---|
| **Minimum energy transferred** | 1 | 2 | 3 | 2 |
| **Continuous evolution of the deformation** | 2 | 1 | 3 | 2 |
| **Deformation homogenization** | 2 | 2 | 3 | 2 |
| **Application on site** | 3 | 2 | 2 | 3 |
| **Cost** | 1 | 3 | 2 | 2 |
| **Mass use** | 1 | 3 | 2 | 2 |
| **Efficiency** | 1 | 2 | 3 | 2 |
| **Total** | 11 | 15 | 18 | 15 |

## References


[1] R. Smilowitz, C. Arnold, M. Ettouney, and M. Kaminskas, "Reference Manual to Mitigate Potential Terrorist Attacks Against Buildings," *Fema 426*, no. October, p. 510, 2011.

[2] G. Secretário-Geral, "Relatório Anual de Segurança Interna," 2016.

[3] T. D. Ngo, P. Mendis, A. Gupta, and J. Ramsay, "Blast Loading and Blast Effects on Structures – An Overview," *Electron. J. Struct. Eng.*, no. January, 2007.

[4] G. Gomes, "Reutilização de edificios correntes para fins operacionais - Blast assessment," Instituto Universitário Militar, 2016.

[5] G. F. Kinney and K. J. Graham, *Explosive Shocks in Air*, 2nd ed. Berlin, Heidelberg, 1985.

[6] D. O. Dusenberry, *Handbook for blast-resistant design of buildins*. New Jersey: John Wiley & Sons, Inc., 2010.

[7] V. Karlos, G. Solomos, and M. Larcher, "Analysis of the blast wave decay coefficient using the Kingery–Bulmash data," *Int. J. Prot. Struct.*, vol. 7, no. 3, 2016.

[8] E. Yandzio and M. Gough, "Protection of Buildings against Explosions," *SCI Publ. 244*, p. 110, 1999.

[9] UNODA, "International Ammunition Technical Guideline (United Nations SaferGuard)," p. 21, 2011.

[10] N. Jones, *Structural impact*. Cambridge, New York: Cambridge University Press, 1989.

[11] C. R. Calladine and R. W. English, "Strain-rate and inertia effects in the collapse of two types of energy-absorbing structure," *Int. J. Mech. Sci.*, vol. 26, no. 11, pp. 689–701, 1984.

[12] T. X. Yut and T. G. Zhang, "A note on a 'Velocity Sensitive' energy-absorbing structure," vol. 8, no. 1, pp. 43–51, 1989.

[13] L. L. Tam and C. R. Calladine, "Inertia and strain-rate effects in a simple plate-structure under impact loading," *Int. J. Impact Eng.*, vol. 11, no. 3, pp. 349–377, 1991.

[14] D. Karagiozova and N. Jones, "Some observations on the dynamic elastic-plastic buckling of a structural model," *Int. J. Impact Eng.*, vol. 16, no. 4, pp. 621–635, 1995.

[15] D. Karagiozova and N. Jones, "A note on the inertia and strain-rate effects in the Tam and Calladine model," *Int. J. Impact Eng.*, vol. 16, no. 4, pp. 637–649, 1995.

[16] X. Y. Su, T. X. Yu, and S. R. Reid, "Inertia-sensitive impact energy-absorbing structures part II: Effect of strain rate," *Int. J. Impact Eng.*, no. 4, pp. 673–689, 1995.

[17] X. Y. Su, T. X. Yu, and S. R. Reid, "Inertia-sensitive impact energy-absorbing structures part I: Effects of inertia and elasticity," *Int. J. Impact Eng.*, vol. 16, no. 4, pp. 651–672, 1995.

[18] A. A. Nassr, A. G. Razaqpur, M. J. Tait, M. Campidelli, and S. Foo, "Strength and stability of steel beam columns under blast load," *Int. J. Impact Eng.*, vol. 55, pp. 34–48, 2013.

[19] A. A. Nassr, A. G. Razaqpur, M. J. Tait, M. Campidelli, and S. Foo, "Experimental performance of steel beams under blast loading," *J. Perform. Constr. Facil.*, vol. 26, no. October, pp. 600–619, 2012.

[20] A. A. Nassr, A. G. Razaqpur, M. J. Tait, M. Campidelli, and S. Foo, "Dynamic Response of Steel Columns Subjected to Blast Loading," *J. Struct. Eng. ASCE*, vol. 140, no. 7, pp. 1–15, 2014.

[21] A. A. Nassr, A. G. Razaqpur, M. J. Tait, M. Campidelli, and S. Foo, "Single and multi degree of freedom analysis of steel beams under blast loading," *Nucl. Eng. Des.*, vol. 242, pp. 63–77, 2012.

[22] S. Guruprasad and A. Mukherjee, "Layred sacrificial claddings under blast loading. Parte I: analytical studies," *Int. J. Impact Eng.*, 2000.